AGU ADVANCING EARTH AND SPACE SCIENCE

Geophysical Research Letters®

RESEARCH LETTER

10.1029/2021GL093966

Key Points:

- Two idealized coupled models, with and without a meridional ocean boundary, show Madden-Julian Oscillation (MJO)- and El Niño-Southern Oscillation (ENSO)-relevant modes of tropical variability
- Zonal asymmetry affects the distinction of an MJO-like intraseasonal mode from equatorial Kelvin waves
- Without the ocean's meridional boundary and the associated ENSO-type dynamics, an interannual mode still persists around the equator

Supporting Information:

Supporting Information may be found in the online version of this article.

Correspondence to:

X. Wu,
xiaoning.wu.1@stonybrook.edu

Citation:

Wu, X., Reed, K. A., Wolfe, C. L. P., Marques, G. M., Bachman, S. D., & Bryan, F. O. (2021). The dependence of tropical modes of variability on zonal asymmetry. *Geophysical Research Letters*, *48*, e2021GL093966. https://doi.org/10.1029/2021GL093966

Received 20 APR 2021
Accepted 23 AUG 2021

The Dependence of Tropical Modes of Variability on Zonal Asymmetry

Xiaoning Wu[1], Kevin A. Reed[1], Christopher L. P. Wolfe[1], Gustavo M. Marques[2], Scott D. Bachman[2], and Frank O. Bryan[2]

[1]School of Marine and Atmospheric Sciences, Stony Brook University, Stony Brook, NY, USA, [2]Climate and Global Dynamics Laboratory, National Center for Atmospheric Research, Boulder, CO, USA

Abstract Tropical modes of variability, including the Madden-Julian Oscillation (MJO) and the El Niño-Southern Oscillation (ENSO), are challenging to represent in climate models. Previous studies suggest their fundamental dependence on zonal asymmetry, but such dependence is rarely addressed with fully coupled ocean dynamics. This study fills the gap by using fully coupled, idealized Community Earth System Model (CESM) and comparing two nominally ocean-covered configurations with and without a meridional boundary. For the MJO-like intraseasonal mode, its separation from equatorial Kelvin waves and the eastward propagation of its convective and dynamic signals depend on the zonal gradient of the mean state. For the ENSO-like interannual mode, in the absence of the ocean's meridional boundary, a circum-equatorial dominant mode emerges with distinct ocean dynamics. The interpretation of the dependence of these modes on zonal asymmetry is relevant to their representation in realistic climate models.

Plain Language Summary In Earth's tropical regions, recurring patterns—such as El Niño and atmospheric waves that come with storm clusters—have a large influence on the global weather and climate. These patterns are also challenging to represent in modern climate models. Previous studies suggest that the behavior of these patterns depends on the east-west contrast in the Pacific ocean, but these studies typically focus on the atmosphere while ignoring relevant actions in the ocean, or vice versa. In this study, we address the question by using a state-of-the-art climate model with a full-blown atmosphere and ocean. We compare two designs with simplified continental shapes, one with east-west contrast and the other without. The behavior of atmospheric waves is more realistic with an east-west contrast. On the other hand, in a global ocean with no land blocking the east-west direction and therefore no east-west contrast, phenomena similar to El Niño can still occur around the equator, but with different ocean processes. Understanding the essential conditions for these patterns will contribute to better climate models for prediction, helping with the preparation for and mitigation of extreme weather and climate events.

1. Introduction

Tropical modes of variability in Earth's climate system, such as the Madden-Julian Oscillation (MJO) and the El Niño-Southern Oscillation (ENSO), have global relevance for climate prediction and projection over various timescales. Yet they remain challenging to represent in state-of-the-art climate models (e.g., Chen et al., 2017; Hung et al., 2013). Over time, model development has generally led to encouraging improvements in their representation (Ahn et al., 2020; G. Wang et al., 2015). However, the complexity of contemporary, full-fledged Earth system models often obscures the sources of improvement (or lack thereof) regarding various aspects or processes (see, e.g., discussion in Bayr et al., 2019; Klingaman & Demott, 2020; Planton et al., 2021). Studying these modes of variability in an idealized framework can facilitate the understanding of their behavior in more complex models. For example, idealized models have been used to study the role of the Pacific mean state—including the zonal gradients in the atmosphere and the ocean—in setting the dynamics of both MJO (e.g., Das et al., 2019; Leroux et al., 2016; Maloney & Wolding, 2015) and ENSO (e.g., Battisti et al., 2019; Clement et al., 2011).

For MJO, a review of its current understanding and modeling challenges is provided by Jiang, Adames, et al. (2020). The role of zonally asymmetric heating by the western Pacific warm pool has been addressed by idealized studies emphasizing the atmospheric component. Through the comparison of atmosphere-only aquaplanet experiments with and without an imposed western warm pool, it is suggested that the zonal asymmetries in both moisture and background mean flow are crucial for realistic features of MJO (Landu & Maloney, 2011; Maloney & Wolding, 2015), although such effects may be model-dependent (Leroux et al., 2016). Das et al. (2019) suggest that the zonal asymmetry in sea surface temperature (SST) is likely more important than the sole presence of continents. Meanwhile, studies using zonally symmetric prescribed SST have explored aspects of sensitivity, including the influences of moisture asymmetry (Hsu et al., 2014), interactive surface evaporation (Shi et al., 2018), and the large-scale background state (Jiang, Maloney, & Su, 2020). On a specific note, although the role of an active ocean component has been suggested for MJO dynamics (e.g., DeMott et al., 2015, and references therein), idealized modeling studies are relatively scarce (e.g., Grabowski, 2006; Maloney & Sobel, 2007, with slab ocean models), and hardly any involve full ocean dynamics.

For ENSO, a brief history of its quintessential dynamic models and outlooks for comprehensive modeling are reviewed in Section 4 of Battisti et al. (2019). With regard to idealization, the first models of ENSO theory and prediction are typically "box-shaped" representations of the Pacific (e.g., Battisti, 1988; Schopf & Suarez, 1988; Zebiak & Cane, 1987). In these classic models with simplified dynamics and minimal physics, the meridional boundary is indispensable for the dynamical adjustment of the equatorial ocean that maintains the interannual oscillation: a sensitivity experiment in Battisti (1988) suggests that the removal of the meridional boundary may result in unconstrained growth of warming, due to the lack of a phase-switching mechanism that counteracts the positive Bjerknes feedback. In contemporary climate models, these ocean dynamics are generally considered necessary for modeling realistic ENSO records (Chen et al., 2017; Planton et al., 2021). On the other hand, reduced-complexity modeling studies have revealed unexpected and intriguing aspects of ENSO-relevant model behaviors affecting interannual timescales, independent of explicit ocean dynamics that require a meridional boundary or zonal asymmetry. For example, studies using slab-ocean models (e.g., Clement et al., 2011; Dommenget et al., 2014) suggest that in the absence of ocean dynamics, feedbacks associated with wind-driven evaporation and cloud radiative effects can lead to realistic ENSO-like behavior in the atmospheric component. Additionally, using a global radiative-convective equilibrium model coupled to a slab ocean—which explicitly excludes zonal asymmetry—Coppin and Bony (2017) suggest that internal variability due to feedbacks between SST and convective aggregation can arise on interannual timescales when the ocean is sufficiently deep. More generally, this behavior is associated with the ocean's role in transferring—or "reddening"—stochastic atmospheric variability on synoptic timescales into climate variability on interannual or longer timescales (e.g., Hasselmann, 1976). Although their existence does not explicitly depend on zonal asymmetry, this type of mechanisms is suggested to affect ENSO (e.g., Perez et al., 2005, using a "box-shaped" simplified Pacific model).

In short, although the fundamental dependence of intraseasonal and interannual modes of tropical variability on zonal asymmetry has been partially addressed by previous works, fully coupled ocean dynamics have generally not been considered. In this study, we explore this question in a fully coupled context. This is done by taking advantage of the newly available idealized and fully coupled configurations of the Community Earth System Model (CESM; Hurrell et al., 2013; Danabasoglu et al., 2020). The design of two idealized configurations and their mean states are documented in detail in Wu et al. (2021, hereafter W21). In the mean state, the zonally asymmetric Ridge configuration—with a single grid-cell-wide meridional boundary for the ocean—is a box-shaped approximation of the Pacific, with the zonal gradient between the western warm pool and eastern cold tongue, and the associated Walker-like circulation. In contrast, the zonally symmetric Aqua configuration—nominally ocean-covered like conventional atmospheric aquaplanets, but coupled to a dynamical ocean—develops a global cold belt of wind-driven equatorial upwelling. For both the intraseasonal and interannual modes, the role of zonal asymmetry is examined in perhaps the most straightforward manner possible by comparing the emergent dynamics when the meridional boundary is present (Ridge) or not (Aqua). Through the exploration, we aim to highlight the aspects through which zonal asymmetry in the mean state affects the MJO- and ENSO-like modes of variability. With an idealized approach, improved understanding of these aspects will have broader relevance for the interpretation and improvement of the representation of these modes of variability in comprehensive, fully coupled models.

10.1029/2021GL093966

2. Model and Data

The two idealized models are configured using CESM (Danabasoglu et al., 2020; Hurrell et al., 2013), with fully coupled atmosphere, ocean, sea ice, and land components. The Ridge configuration (similar to Enderton & Marshall, 2009; Smith et al., 2006) is zonally bounded by a single strip of pole-to-pole continent along the prime meridian. The Aqua configuration, without the meridional boundary, is nominally ocean-covered and zonally symmetric. Both configurations have two minimal polar caps required by the ocean grid. All land is flat.

The model design is described in detail in W21. By Year 400, both models reach quasi-equilibrium climate states (see W21 for details). Due to computational and storage constraints for archiving model outputs at high temporal resolution, the results in Section 3.1 are based on 6-hourly output of the atmosphere over the 20-year record of Year 401–420. The results in Section 3.2 use monthly averaged output of the atmosphere and annually averaged output of the ocean over the 100-year record of Year 401–500.

3. Results

3.1. Convectively Coupled Equatorial Waves and Intraseasonal Variability

The Ridge configuration captures a range of features of convectively coupled equatorial waves (CCEWs) and MJO qualitatively consistent with Earth observations. Figure 1 shows the vertical profiles of climatological zonal wind averaged between 15°N–15°S, and Wheeler-Kiladis diagrams (Wheeler & Kiladis, 1999) based on 6-hourly precipitation. Throughout most vertical levels, Ridge's background zonal flow is relatively weak at ~– 5 m s^{-1} or lower (Figure 1a). Therefore, the zero-mean-flow approximation typical for the dispersion relations of CCEWs in the Wheeler-Kiladis diagrams is reasonably adequate (solid black curves in Figures 1b and 1d). In the symmetric component (Figure 1b), spectral signals corresponding to equatorial Rossby and Kelvin waves are present. An MJO-like mode reaching zonal wave numbers 3–4 is separated from the dispersion relation of equatorial Kelvin waves with periodicity beyond 20 days (dark blue box in Figure 1b). In the antisymmetric component (Figure 1d), signals corresponding to mixed Rossby-gravity and inertia-gravity waves are also present.

Focusing on the MJO-like mode, Figure 2 shows its propagation embedded in the mean state. The climatological precipitation of the Ridge configuration (Figure 2a) is shaped by the climatological SST (Figure 2f in W21). Two ITCZs converge toward the western warm pool, and the relatively dry region over the eastern cold tongue reflects the descending branch of the Walker-like circulation (Figure 2b in W21). Following Waliser et al. (2009), the MJO-like mode is extracted by band pass filtering the precipitation and low-level zonal wind at 850 hPa to retain only motions with periods between 20 and 100 days. The propagation of this mode is then examined using lagged correlation across both the zonal (Figure 2c) and meridional (Figure 2e) directions. The reference region of the lagged correlation, marked by the orange box in Figure 2a, is chosen on the western side of the climatological warm pool, loosely analogous to the Indian Ocean for observed MJO (Ahn et al., 2017; Waliser et al., 2009). In the zonal direction (Figure 2c), the intraseasonal precipitation anomaly shows coherent eastward propagation over local centers of maximum climatological precipitation near 90°E around the climatological warm pool before decaying. The dynamic anomaly, as represented by intraseasonal low-level zonal wind, lags behind the precipitation anomaly by ~5 days west of ~90°E. As the precipitation anomaly decays east of ~90°E, the zonal wind anomaly shows increased phase speed over the drier region. In the meridional direction (Figure 2e), both the precipitation anomaly and the zonal wind anomaly show poleward propagation. The poleward propagation is enhanced in the summer hemisphere, as the ITCZ shifts seasonally (see Figure S1). The equatorward contraction of the centers of maximum lagged correlation in precipitation (Figure 2e) reflects the zonal structure of the underlying climatology. These characteristics are qualitatively consistent with the propagation of observed MJO over the Pacific (cf., Figures 5 and 6 in Waliser et al. [2009]). It is also worth mentioning that the qualitative features of the lagged correlation discussed above are not sensitive to the exact longitude of the reference region in Figure 2a, as long as its general position relative to the climatological warm pool is maintained.

In the Aqua configuration where zonal asymmetry is removed, the intraseasonal variability—as well as the rest of CCEWs—are notably affected. Aqua's background easterly flow is substantially stronger than Ridge

10.1029/2021GL093966

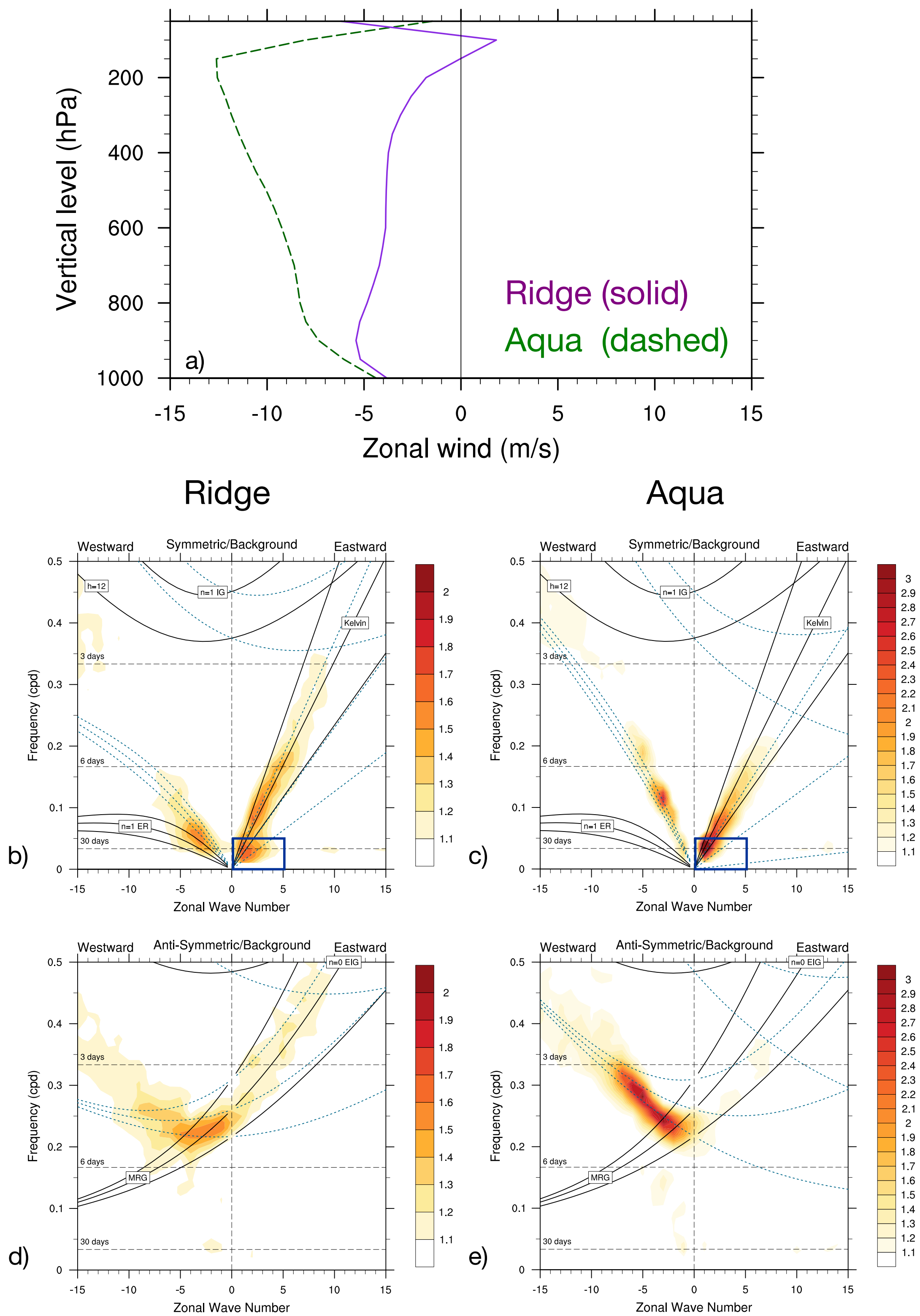

Figure 1. The interaction between the zonal mean flow and convectively coupled equatorial waves, using data from Yr 401–420. (a) Vertical profiles of the zonal mean zonal wind, averaged between 15°N and 15°S. (b–e) Wheeler-Kiladis diagrams of 6-hourly precipitation, averaged between 15°N and 15°S. The solid black curves represent the theoretical dispersion relations assuming zero zonal flow, whereas the dashed blue curves represent the dispersion relations Doppler-shifted by the background zonal flow of $-5\ \mathrm{m\ s^{-1}}$ for Ridge (b and d), and $-10\ \mathrm{m\ s^{-1}}$ for Aqua (c and e).

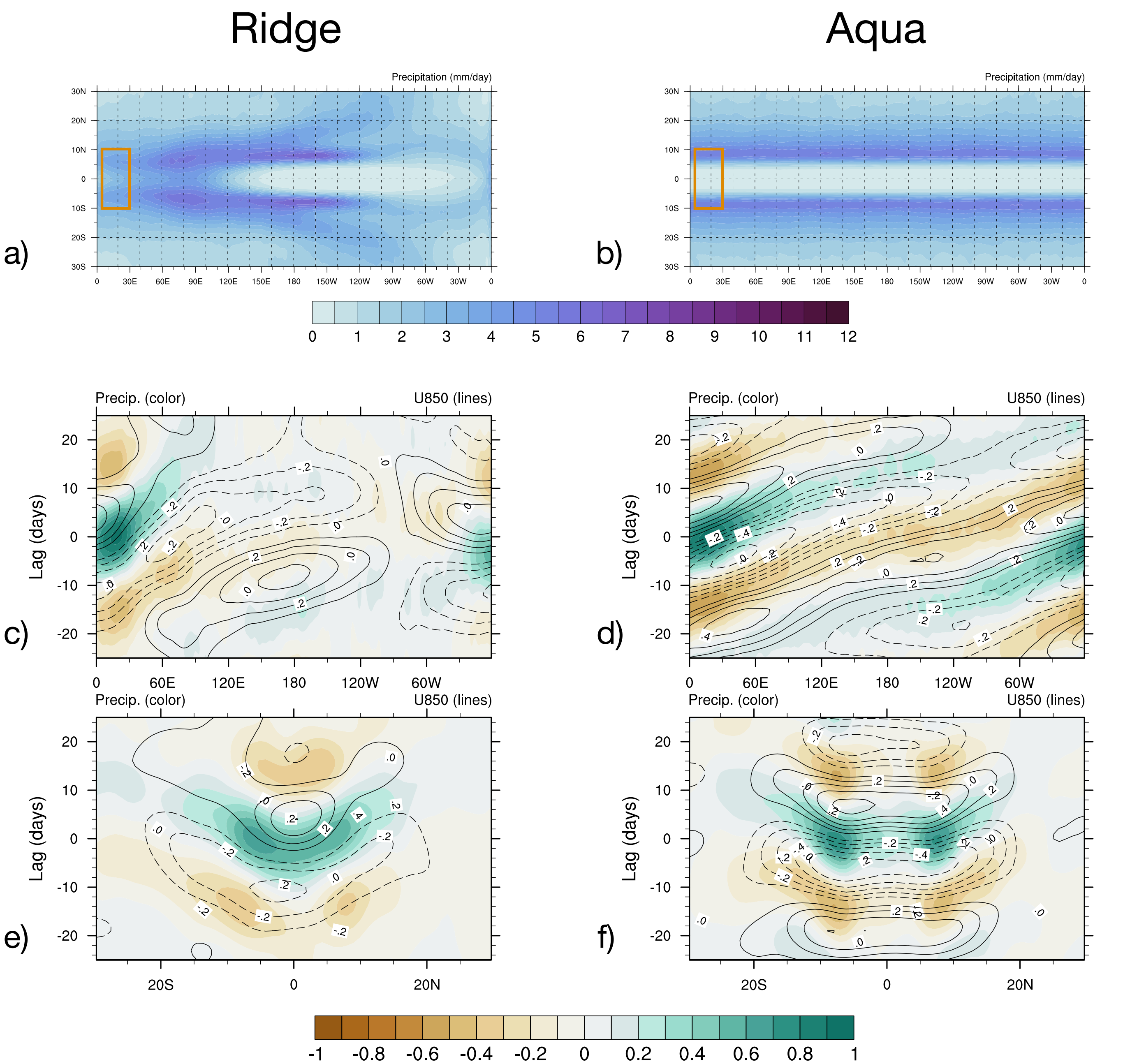

Figure 2. The propagation of the Madden-Julian Oscillation (MJO)-like mode, using data from Yr 401–420. (a and b) The climatology of annual average precipitation (mm day^{-1}). (c–f) Lagged correlation of the filtered signal with 20–100 day period in precipitation (colored shading) and low-level zonal wind at 850 hPa (contour line), across the zonal direction (c–d) and meridional direction (e–f). The orange box of 10°N–10°S, 5°–30°E in panels (a and b) marks the reference location of the lagged correlation in panels (c–f).

throughout almost all the vertical levels, reaching beyond ~− 10 m s^{-1} in the upper levels (Figure 1a). As a result, in the Wheeler-Kiladis diagrams (Figures 1c and 1e), the westward signals are not well approximated by the theoretical dispersion relations of equatorial Rossby or mixed Rossby-gravity waves assuming zero background velocity. This is largely due to Doppler-shifting by the background zonal flow (e.g., regional observation discussed by Dias and Kiladis [2014]), that is, the frequency $\hat{\omega}$ of motions observed in an Eulerian frame is different from the true frequency, ω, in the presence of a nonzero background velocity, $\mathbf{U}$ (see e.g., Ch. 11 in Gill [1982]):

$$\hat{\omega} = \omega - \mathbf{U} \cdot \mathbf{k}. \tag{1}$$

10.1029/2021GL093966

Accounting for the background flow by incorporating a zonal velocity of -10 m s^{-1}, dispersion relations are generated that align with the empirical signals (dashed blue curves in Figures 1c and 1e). In comparison to Aqua (Figures 1c and 1e), a background mean flow of -5 m s^{-1} is incorporated for Ridge (dashed blue curves in Figures 1b and 1d) to demonstrate the smaller effects arising from the mean easterly flow. Note that for either configuration, the magnitude of the background zonal velocity is a qualitative indication rather than a precise estimate (see e.g., discussion in Dias and Kiladis [2014], on the considerations for such estimates). For Aqua's intraseasonal variability with periodicity beyond 20 days (dark blue box in Figure 1c), its dispersion characteristics becomes much less distinct from equatorial Kelvin waves than in the Ridge configuration, with reduced zonal wave numbers.

For comparison, Aqua's intraseasonal variability is diagnosed in the same manner as the Ridge configuration in Figure 2, although its behavior is more consistent with convectively coupled Kelvin waves than with MJO. As discussed in W21, the climatological precipitation of the Aqua configuration (Figure 2b) shows two ITCZs around 10°N/S that correspond to the locations of SST maxima, and a cold and dry equatorial belt where precipitation is suppressed by the descending branch of the "reverse Hadley" circulation (see Figures 4b and 8a in W21). Given the zonal uniformity of the Aqua configuration, the longitude of the reference region for the lagged correlation is entirely arbitrary, and coordinates identical to that of the Ridge configuration are used (the orange box in Figure 2b). In the zonal direction (Figure 2d), the propagation of the precipitation anomaly likewise leads the zonal wind anomaly by ~5 days. The contrast with Ridge is in line with what the mean state might imply: without the zonal gradient in moisture, the phase speed of the zonal wind anomaly becomes nearly zonally uniform, and the propagation of precipitation anomaly becomes more persistent. In the meridional direction (Figure 2f), both of the anomalies likewise propagate poleward, and without Ridge's zonal structure, the centers of maximum lagged correlation in precipitation remain around the latitude of the climatological double ITCZs.

The comparison above suggests dynamic and thermodynamic aspects through which zonal asymmetry affects CCEWs and the MJO-like intraseasonal mode. For CCEWs, Aqua's zonal symmetry produces stronger background mean easterlies in the tropics, leading to more pronounced Doppler-shifting in the dispersion relations. For the MJO-like intraseasonal mode, Ridge's zonal structure of the thermodynamic environment in the mean state is essential for the dynamic and convective structure of this mode. These factors likely affect the separation of this mode from equatorial Kelvin waves: in the Ridge configuration its spatial scale is constrained by the climatological warm pool, whereas in Aqua's zonally uniform double ITCZs, this spatial constraint is removed, resulting in reduced zonal wave numbers.

3.2. Equatorial Mode of Interannual Variability

It is perhaps not surprising that the interannual variability of the Ridge configuration is dominated by an ENSO-like equatorial mode. Figure 3 shows the empirical features of this dominant mode. In the first empirical orthogonal function (EOF) of monthly SST after removing the climatological seasonal cycle and long-term linear trend (Figure 3a), the region with maximum variance is in the climatological cold tongue on the eastern side of the basin (cf., Figure 2f in W21). In analogy to regions of Niño SST indices in the Pacific, an indicative region is marked by the dashed blue box in Figure 3a. The selection of this region is based on the pattern of SST variance, which also largely encompasses the climatological cold tongue with colder SST than the zonal average (cf., Figure 2h in W21). As expected from the EOF methodology, the first principle component is closely associated with the average SST anomaly of this region (Figure 3c). The SST composite of warming years is shown in Figure S2a. The periodicity of the monthly averaged SST anomaly is in the range of 1.5–3 years (Figure 3e). The monthly averaged SST anomaly ranges between -2.50–2.96°C, with standard deviation of 0.77°C and skewness of 0.15. The skewness toward warming qualitatively captures the observed feature of ENSO asymmetry (e.g., An & Jin, 2004). Notably, given the hemispheric symmetry of the model, the variance of monthly average SST anomaly in this indicative region peaks in both the boreal summer and winter seasons. The phase-locking to both seasons—instead of only boreal winter in the Pacific—likely contributes to the shorter period of this interannual mode, despite Ridge's basin size being wider than the Pacific.

Geophysical Research Letters

10.1029/2021GL093966

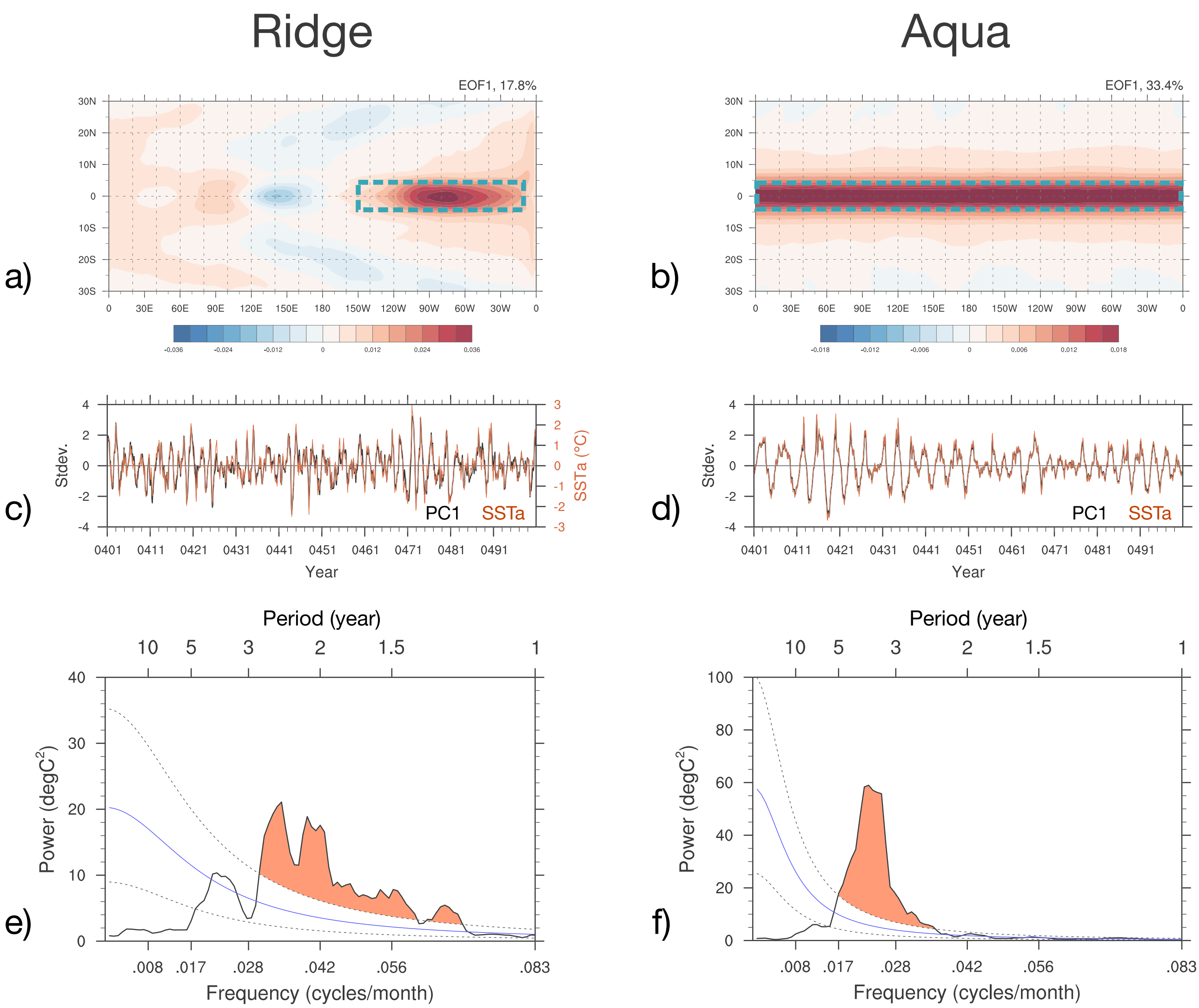

Figure 3. The leading mode of interannual variability in the equatorial region, using monthly averaged SST from Yr 401–500. The data is linearly detrended, and the climatological seasonal cycle is removed. (a and b) The first EOF (normalized with spatial variance of unity), where the dashed blue box marks the equatorial region of dominating variability, 5°N–5°S, 150°W–10°W for Ridge (a) and 5°N–5°S for Aqua (b). (c and d) Time series of monthly SST anomaly (red) averaged over the boxed region in (a and b), and the standardized first PC (black). (e and f) The power spectra of the SST time series. The orange shading indicates significant spectral peaks beyond 95% confidence level (i.e., $p < 0.05$).

An exploration of these ENSO-like events in the Ridge configuration suggests processes comparable to the Pacific. Figure 4 shows the ocean composite of warming years, and the strength of SST feedbacks as suggested by Planton et al. (2021). Using annually averaged ocean model output, the warming (cooling) years are defined as years where the annually averaged SST anomaly in the indicative region exceeds (drops below) one standard deviation. In the 100-year record, there are 17 warming years and 15 cooling years. The warming-year composite of sub-surface temperature anomaly 5°N–5°S is shown in Figure 4a. On the eastern side of the basin, the near-surface warming reaches down to ~100 m near the center of maximum warming around 90 W, and to ~300 m near the eastern boundary. On the western side of the basin, the sub-surface cooling along the climatological thermocline (cf., Figure 2j in W21) suggests classical mechanisms for ENSO phase-switching (see e.g., review by C. Wang [2018]).

The strength of the feedback between SST and zonal wind stress—or the Bjerknes feedback—is shown in Figure 4c. As in the Pacific, positive SST anomaly in the indicative region corresponds to relaxed easterly wind stress around the equator 180°–90°W (cf., Figure 2d in W21). The strength of the feedback between SST and surface heat flux is shown in Figure 4e. East of 90°W, positive SST anomaly in the indicative

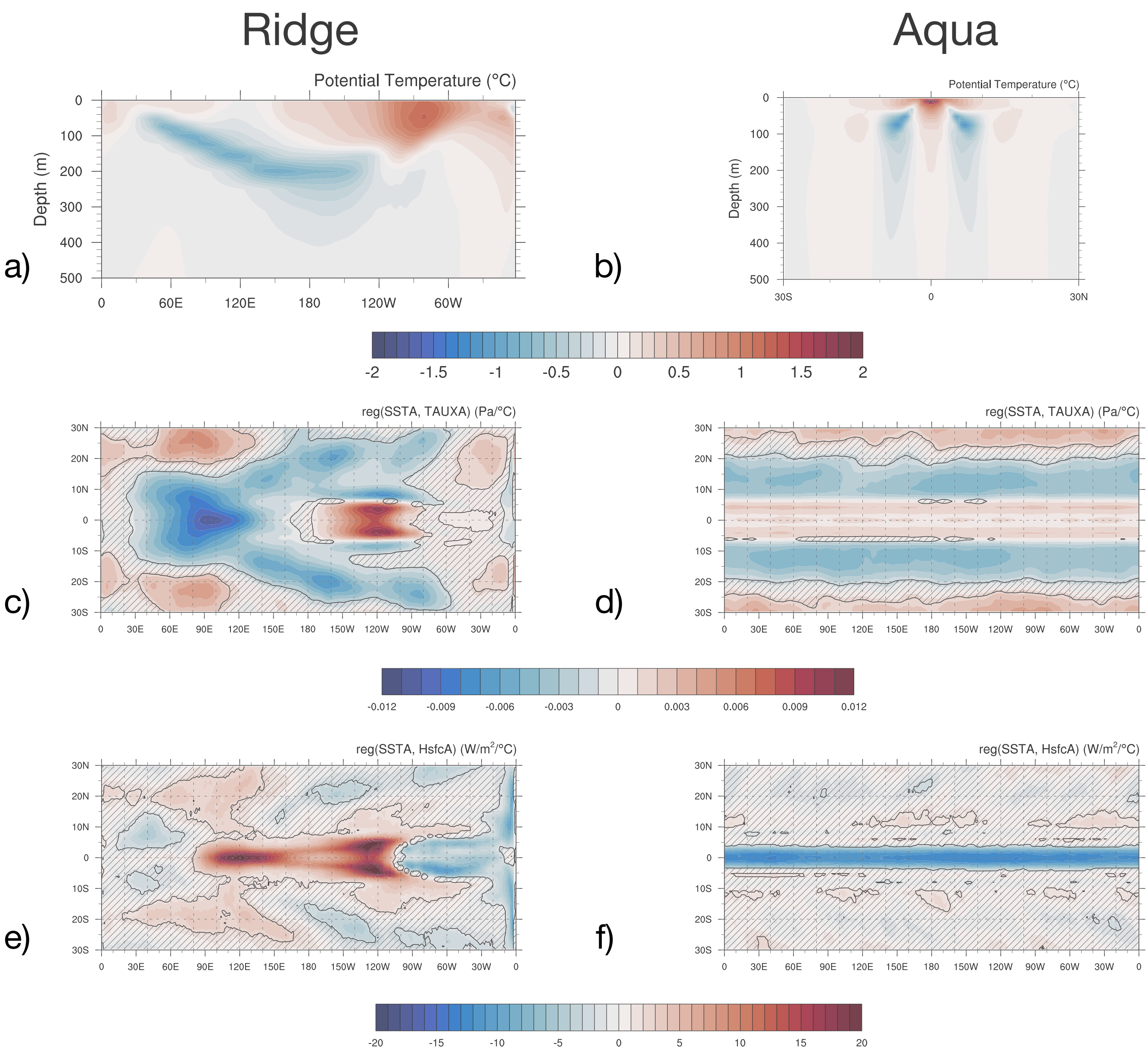

Figure 4. Composites of interannual warming events and SST feedbacks, using monthly averaged atmospheric data and annually averaged ocean potential temperature from Yr 401–500. The data is linearly detrended, and the climatological seasonal cycle is removed. (a and b) The composite of upper-ocean potential temperature anomaly of warming years (see text for definition), meridionally averaged 5°N–5°S to show the zonal structure for Ridge (a), and zonally averaged to show the meridional structure between 30°N and 30°S for Aqua (b). (c and d) The strength of SST-zonal wind stress feedback, measured by the regression of SST anomaly on zonal wind stress anomaly. (e and f) The strength of SST-surface heat flux feedback, measured by the regression of SST anomaly on surface heat flux anomaly. The hatched areas in panels (c–f) mask out correlations below 95% confidence level (i.e., $p \geq 0.05$).

regions corresponds to decreased surface heat flux into the ocean. On the other hand, the feedback is positive west of 90°W. This pattern largely comes from the combination of shortwave and latent heat anomalies (see Figure S3 for components of surface heat flux). East of 100°W, where the wind stress anomaly is small (Figure 4c), the positive SST anomaly enhances the latent heat flux into the atmosphere (Figure S3e). Meanwhile, the relaxation of the easterlies west of 100°W likely contributes to the reduction of latent heat flux into the atmosphere, therefore warming the ocean. The opposing feedbacks in radiation, positive for shortwave and negative for longwave (Figures S3a and S3c), suggest the role of clouds.

By design, the zonally symmetric Aqua configuration lacks the meridional boundary essential for aspects of ENSO dynamics related to oceanic wave reflection in the zonal direction. Somewhat surprisingly, its interannual variability is likewise dominated by an equatorial mode over the climatological cold belt of upwelling (Figure 3b; cf., Figure 2e in W21). Here the indicative region is extended accordingly (dashed blue box in Figure 3b). The time series of SST anomaly varies at lower frequency than the Ridge configuration (Figure 3d), with periodicity of 2–5 years (Figure 3f). The average SST anomaly ranges between – 2.68 –2.55°C, with standard deviation of 0.81°C. Interestingly, with skewness of – 0.12, this equatorial mode of the Aqua configuration skews toward cooling. For the seasonal phase-locking, like the Ridge configuration, the variance of monthly average SST anomaly in the indicative region is bimodal in the annual cycle, peaking in both the summer and winter seasons.

As can be expected from the mean state (cf., Section 3.2 in W21), the ocean dynamics associated with this mode are substantially different from its ENSO-like counterpart in the Ridge configuration. Using the same definition for the annually averaged SST in the indicative region, there are 16 warming years and 16 cooling years in the 100-year record. To focus on the meridional structure, the warming-year composite of sub-surface temperature anomaly is zonally averaged (Figure 4a). Very near to the equator in the latitude band 2°N–2°S, the near-surface warming reaches beyond ~100 m. In the off-equatorial region 2–10°N/S, there is sub-surface cooling reaching beyond ~300 m. The persistence of these sub-surface cold anomalies through the annual cycle is likely essential for the phase-switching on the interannual time scale. As discussed in W21, since there is no geostrophically balanced meridional flow in the ocean interior for the Aqua configuration, meridional advection is attributed to parameterized eddy processes. The equatorward advection from ~5–10°N/S by meridional eddy velocity of ~$O(1)$ cm s^{-1} yields a timescale of ~2–4 years, which likely contributes to the interannual phase-switching of this mode (cf., Figure 8c in W21 for the residual overturning circulation).

On the other hand, despite the contrast in the ocean interior, some aspects of the atmospheric component of Aqua's interannual mode may be meaningfully compared to that of the Ridge configuration over the eastern side of the basin. Figure 4d indicates the positive feedback between SST and zonal wind stress over the equatorial region 5°N–5°S. Although the regression here does not directly resolve the question of causality, the positive feedback can be reasonably expected. Warm SST anomalies in the cold belt, by reducing the meridional SST gradient, would lead to reduced off-equatorial easterly wind stress via geostrophic adjustment; meanwhile, reduced off-equatorial easterly wind stress is conducive to warmer equatorial SST via reduced upwelling. This positive feedback works to qualitatively similar effects as the canonical Bjerknes feedback, albeit impacting the meridional SST gradient instead of zonal. For the coupling between SST and surface heat flux anomalies (Figure 4f), the negative feedback over the equatorial region is mostly through latent heat (Figure S3f), where warmer equatorial SST enhances the latent heat flux into the atmosphere, and the relaxation of zonal wind by relatively small magnitude does not significantly counter this effect. In this aspect, Aqua's equatorial cold belt may be regarded as behaving similarly to the eastern part of Ridge's cold tongue east of 100°W (Figure 4e). The opposing feedbacks in shortwave and longwave (Figures S3b and S3d), making a relatively small contribution, take effect over the regions of climatological off-equatorial SST maxima (Figure 4a in W21). These regions correspond to the ascending branch of the Hadley-like cells, conducive for clouds (Figure 4d in W21).

In summary, the Ridge configuration is a reasonable model of the Pacific for both the mean state and its ENSO-like interannual variability, with characteristics and feedback processes relevant to realistic models. Similar variability exists in the Aqua model despite the lack of a meridional boundary. Contrary to Ridge's zonal structure, Aqua's essential ocean dynamics occur in the meridional direction, where off-equatorial subsurface temperature anomalies of opposite sign to the near-surface anomalies are likely important for the phase-switching. Such mechanisms involving the sub-surface anomalies in the meridional direction may be part of observed ENSO processes (e.g., "trade wind charging" in Anderson et al. [2013] and Chakravorty et al. [2020]). SST feedbacks over Ridge's eastern cold tongue are partially maintained in Aqua's equatorial cold belt, although with different mechanisms. The contrast suggests that for some of these ENSO-relevant processes, their maintenance are not necessarily dependent on the zonal asymmetry resulting from the ocean's meridional boundary. Besides the relevance for the modern-day Pacific, these processes may be particularly relatable to paleoclimate variability where the equatorial region had less extensive land barriers (e.g., Davies et al., 2011, 2012).

4. Discussion

Building on insights from previous works, fully coupled idealized models with resolution and physics similar to CMIP-class models are employed to investigate the dependence of MJO- and ENSO-like modes of variability on zonal asymmetry. We discuss the following aspects in the context of previous studies.

For the intraseasonal mode, when fully coupled ocean dynamics are included, the role of zonal asymmetry in enhancing more realistic MJO structures is mostly consistent with previous atmosphere-only idealized studies (Das et al., 2019; Landu & Maloney, 2011; Maloney & Wolding, 2015). However, somewhat contrary to the suggestion by Jiang, Maloney, and Su (2020), the propagation of the intraseasonal variability is not necessarily prohibited by the presence of double ITCZs in either the Ridge or Aqua configurations. Aside from model-dependent details in the atmospheric component, it remains to be seen if the interactive ocean coupling may have affected the propagation. More generally, the essential dynamics of MJO have been long debated (see the review of theories by Jiang, Adames, et al. [2020]), including moisture modes (e.g., Adames & Kim, 2016; Shi et al., 2018) or variant forms of tropical waves (e.g., Kim & Zhang, 2021; Roundy, 2012; Yang & Ingersoll, 2013). Based on the contrast between the current Ridge and Aqua models, additional process-level diagnostics will likely provide more detailed perspectives on the distinction of this mode from Kelvin waves as represented in comprehensive climate models.

For the interannual mode, its existence in the equatorial cold belt on the coupled CESM Aqua planet prompts questions on model dependency. As reviewed in W21, the documentation of fully coupled idealized models is rare, and the discussion on variability even more scarce. Of the only other known documentation on this topic, the coupled Aqua model in Marshall et al. (2007) shows a leading mode of variability in the midlatitudes instead of the tropics. Considering the abundance of differences in the model configuration, the resulting differences in variability again suggest the role of the mean state (e.g., the intensity of equatorial upwelling and the associated atmospheric circulation) in constraining the variability. For other zonally bounded Ridge models with Aqua counterparts, the discussion on whether an ENSO-like mode of interannual variability is present has so far not been documented (Farneti & Vallis, 2009; Marshall et al., 2007; Smith et al., 2006). It is worth considering the potential links between the Aqua and Ridge modes of interannual variability, with implications for representing ENSO in realistic Earth configurations.

As concluding thoughts, we suggest a few future directions stemming from this exploratory work in the idealized, coupled modeling framework. For the MJO-like intraseasonal mode, its mechanisms in the Ridge model (and apparent lack thereof in Aqua) can be further discerned by diagnosing the moist static energy budget. In addition, the role of the large-scale SST structure versus active ocean coupling can be isolated by prescribed-SST experiments, in comparison to previous atmosphere-only idealized studies. For the ENSO-like interannual mode, the representation of relevant processes for its initiation and maintenance—including those suggested by the "delayed oscillator" and related theories (e.g., Jin, 1997; Schopf & Suarez, 1988; Weisberg & Wang, 1997)—can be further understood by diagnosing the upper ocean heat budget, and the corresponding atmospheric interactions. Moreover, an extension of the current model hierarchy can help clarify the fundamental controls for the seasonal phase-locking by opening up the Drake Passage of Ridge and introducing interhemispheric asymmetry. For these suggested directions, the simplicity of idealized configurations can uniquely facilitate these types of experiments and the interpretation of dynamical impacts. Furthermore, with increased model resolution, a wider range of scale interactions may be explored, including tropical cyclones.

Data Availability Statement

The CESM Aqua and Ridge model case directories and the simulation outputs are available at https://doi.org/10.5281/zenodo.4646251, and on CISL's Globally Accessible Data Environment. The CESM source code is available at https://github.com/ESCOMP/CESM. The first author dedicates this manuscript to the victims and responding officer fallen to the mass shooting at our neighborhood grocery store in Boulder, CO in March 2021.

Acknowledgments

The authors thank Antonietta Capotondi, Hyemi Kim, Sarah Larson, Levi Silvers, Christine Shields, Bette Otto-Bliesner, and many others for helpful discussions. The authors also thank an anonymous reviewer whose constructive comments helped us improve this manuscript. The analysis of CCEWs benefited from diagnostic tools authored by Carl Schreck, provided at https://ncics.org/portfolio/monitor/mjo/. X. Wu was supported by National Science Foundation (NSF) grant AGS1648629, the Advanced Study Program of NCAR, and the Junior Researcher Award of the Institute for Advanced Computational Science at Stony Brook University. Reed was supported by NSF grants AGS1648629 and AGS1830729. The National Center for Atmospheric Research (NCAR) is sponsored by the NSF under Cooperative Agreement 1852977. The authors acknowledge computing and data storage resources, including the Cheyenne supercomputer (https://doi.org/10.5065/D6RX99HX), provided by the Computational and Information Systems Laboratory (CISL) at NCAR. The first author dedicates this manuscript to the victims and responding officer fallen to the mass shooting at our neighborhood grocery store in Boulder, CO in March 2021.

References

Adames, Á. F., & Kim, D. (2016). The MJO as a dispersive, convectively coupled moisture wave: Theory and observations. *Journal of the Atmospheric Sciences*, *73*(3), 913–941. https://doi.org/10.1175/jas-d-15-0170.1

Ahn, M.-S., Kim, D., Kang, D., Lee, J., Sperber, K. R., Gleckler, P. J., & Kim, H. (2020). MJO propagation across the maritime continent: Are CMIP6 models better than CMIP5 models? *Geophysical Research Letters*, *47*(11), e2020GL087250. https://doi.org/10.1029/2020gl087250

Ahn, M.-S., Kim, D., Sperber, K. R., Kang, I.-S., Maloney, E., Waliser, D., & Hendon, H. (2017). MJO simulation in CMIP5 climate models: MJO skill metrics and process-oriented diagnosis. *Climate Dynamics*, *49*(11), 4023–4045. https://doi.org/10.1007/s00382-017-3558-4

An, S.-I., & Jin, F.-F. (2004). Nonlinearity and asymmetry of ENSO. *Journal of Climate*, *17*(12), 2399–2412. https://doi.org/10.1175/1520-0442(2004)017<2399:naaoe>2.0.co;2

Anderson, B. T., Perez, R. C., & Karspeck, A. (2013). Triggering of El Niño onset through trade wind–induced charging of the equatorial Pacific. *Geophysical Research Letters*, *40*(6), 1212–1216. https://doi.org/10.1002/grl.50200

Battisti, D. S. (1988). Dynamics and thermodynamics of a warming event in a coupled tropical atmosphere–ocean model. *Journal of Atmospheric Sciences*, *45*(20), 2889–2919. https://doi.org/10.1175/1520-0469(1988)045<2889:datoaw>2.0.co;2

Battisti, D. S., Vimont, D. J., & Kirtman, B. P. (2019). 100 years of progress in understanding the dynamics of coupled atmosphere–ocean variability. *Meteorological Monographs*, *59*, 8.1–8.57. https://doi.org/10.1175/amsmonographs-d-18-0025.1

Bayr, T., Wengel, C., Latif, M., Dommenget, D., Lübbecke, J., & Park, W. (2019). Error compensation of ENSO atmospheric feedbacks in climate models and its influence on simulated ENSO dynamics. *Climate Dynamics*, *53*(1), 155–172. https://doi.org/10.1007/s00382-018-4575-7

Chakravorty, S., Perez, R. C., Anderson, B. T., Giese, B. S., Larson, S. M., & Pivotti, V. (2020). Testing the trade wind charging mechanism and its influence on ENSO variability. *Journal of Climate*, *33*(17), 7391–7411. https://doi.org/10.1175/jcli-d-19-0727.1

Chen, C., Cane, M. A., Wittenberg, A. T., & Chen, D. (2017). ENSO in the CMIP5 simulations: Life cycles, diversity, and responses to climate change. *Journal of Climate*, *30*(2), 775–801. https://doi.org/10.1175/jcli-d-15-0901.1

Clement, A., DiNezio, P., & Deser, C. (2011). Rethinking the ocean's role in the Southern Oscillation. *Journal of Climate*, *24*(15), 4056–4072. https://doi.org/10.1175/2011jcli3973.1

Coppin, D., & Bony, S. (2017). Internal variability in a coupled general circulation model in radiative-convective equilibrium. *Geophysical Research Letters*, *44*(10), 5142–5149. https://doi.org/10.1002/2017gl073658

Danabasoglu, G., Lamarque, J.-F., Bacmeister, J., Bailey, D., DuVivier, A., Edwards, J., et al. (2020). The Community Earth System Model version 2 (CESM2). *Journal of Advances in Modeling Earth Systems*, *12*(2), e2019MS001916. https://doi.org/10.1029/2019ms001916

Das, S., Sengupta, D., & Chakraborty, A. (2019). The Madden-Julian Oscillation in an aquaplanet-like general circulation model with and without continents. *Journal of Advances in Modeling Earth Systems*, *11*(5), 1459–1476. https://doi.org/10.1029/2018ms001455

Davies, A., Kemp, A. E., & Pälike, H. (2011). Tropical ocean-atmosphere controls on inter-annual climate variability in the Cretaceous Arctic. *Geophysical Research Letters*, *38*(3). https://doi.org/10.1029/2010gl046151

Davies, A., Kemp, A. E., Weedon, G. P., & Barron, J. A. (2012). El Niño–southern oscillation variability from the late cretaceous Marca shale of California. *Geology*, *40*(1), 15–18. https://doi.org/10.1130/g32329.1

DeMott, C. A., Klingaman, N. P., & Woolnough, S. J. (2015). Atmosphere-ocean coupled processes in the Madden-Julian Oscillation. *Reviews of Geophysics*, *53*(4), 1099–1154. https://doi.org/10.1002/2014rg000478

Dias, J., & Kiladis, G. N. (2014). Influence of the basic state zonal flow on convectively coupled equatorial waves. *Geophysical Research Letters*, *41*(19), 6904–6913. https://doi.org/10.1002/2014gl061476

Dommenget, D., Haase, S., Bayr, T., & Frauen, C. (2014). Analysis of the Slab Ocean El Nino atmospheric feedbacks in observed and simulated ENSO dynamics. *Climate Dynamics*, *42*(11), 3187–3205. https://doi.org/10.1007/s00382-014-2057-0

Enderton, D., & Marshall, J. (2009). Explorations of atmosphere–ocean–ice climates on an aquaplanet and their meridional energy transports. *Journal of the Atmospheric Sciences*, *66*(6), 1593–1611. https://doi.org/10.1175/2008jas2680.1

Farneti, R., & Vallis, G. (2009). An Intermediate Complexity Climate Model (ICCMp1) based on the GFDL flexible modelling system. *Geoscientific Model Development*, *2*(2), 73–88. https://doi.org/10.5194/gmd-2-73-2009

Gill, A. E. (1982). *Atmosphere—Ocean dynamics*. Elsevier.

Grabowski, W. W. (2006). Impact of explicit atmosphere–ocean coupling on MJO-like coherent structures in idealized aquaplanet simulations. *Journal of the Atmospheric Sciences*, *63*(9), 2289–2306. https://doi.org/10.1175/jas3740.1

Hasselmann, K. (1976). Stochastic climate models Part I. Theory. *Tellus*, *28*(6), 473–485. https://doi.org/10.3402/tellusa.v28i6.11316

Hsu, P.-C., Li, T., & Murakami, H. (2014). Moisture asymmetry and MJO eastward propagation in an aquaplanet general circulation model. *Journal of Climate*, *27*(23), 8747–8760. https://doi.org/10.1175/jcli-d-14-00148.1

Hung, M.-P., Lin, J.-L., Wang, W., Kim, D., Shinoda, T., & Weaver, S. J. (2013). MJO and convectively coupled equatorial waves simulated by CMIP5 climate models. *Journal of Climate*, *26*(17), 6185–6214. https://doi.org/10.1175/jcli-d-12-00541.1

Hurrell, J. W., Holland, M. M., Gent, P. R., Ghan, S., Kay, J. E., Kushner, P. J., et al. (2013). The Community Earth System Model: A framework for collaborative research. *Bulletin of the American Meteorological Society*, *94*(9), 1339–1360. https://doi.org/10.1175/bams-d-12-00121.1

Jiang, X., Adames, Á. F., Kim, D., Maloney, E. D., Lin, H., Kim, H., & Klingaman, N. P. (2020). Fifty years of research on the Madden-Julian Oscillation: Recent progress, challenges, and perspectives. *Journal of Geophysical Research: Atmospheres*, *125*(17), e2019JD030911. https://doi.org/10.1029/2019jd030911

Jiang, X., Maloney, E., & Su, H. (2020). Large-scale controls of propagation of the Madden-Julian Oscillation. *npj Climate and Atmospheric Science*, *3*(1), 1–8. https://doi.org/10.1038/s41612-020-00134-x

Jin, F.-F. (1997). An equatorial ocean recharge paradigm for ENSO. Part I: Conceptual model. *Journal of the Atmospheric Sciences*, *54*(7), 811–829. https://doi.org/10.1175/1520-0469(1997)054<0811:aeorpf>2.0.co;2

Kim, J.-E., & Zhang, C. (2021). Core dynamics of the MJO. *Journal of the Atmospheric Sciences*, *78*(1), 229–248. https://doi.org/10.1175/jas-d-20-0193.1

Klingaman, N. P., & Demott, C. A. (2020). Mean state biases and interannual variability affect perceived sensitivities of the Madden-Julian Oscillation to air-sea coupling. *Journal of Advances in Modeling Earth Systems*, *12*(2), e2019MS001799. https://doi.org/10.1029/2019ms001799

Landu, K., & Maloney, E. D. (2011). Effect of SST distribution and radiative feedbacks on the simulation of intraseasonal variability in an aquaplanet GCM. *Journal of the Meteorological Society of Japan. Ser. II*, *89*(3), 195–210. https://doi.org/10.2151/jmsj.2011-302

10.1029/2021GL093966

Leroux, S., Bellon, G., Roehrig, R., Caian, M., Klingaman, N. P., Lafore, J.-P., et al. (2016). Inter-model comparison of subseasonal tropical variability in aquaplanet experiments: Effect of a warm pool. *Journal of Advances in Modeling Earth Systems*, *8*(4), 1526–1551. https://doi.org/10.1002/2016ms000683

Maloney, E. D., & Sobel, A. H. (2007). Idealized hot spot experiments with a general circulation model. *Journal of Climate*, *20*(5), 908–925. https://doi.org/10.1175/jcli4053.1

Maloney, E. D., & Wolding, B. O. (2015). Initiation of an intraseasonal oscillation in an aquaplanet general circulation model. *Journal of Advances in Modeling Earth Systems*, *7*(4), 1956–1976. https://doi.org/10.1002/2015ms000495

Marshall, J., Ferreira, D., Campin, J.-M., & Enderton, D. (2007). Mean climate and variability of the atmosphere and ocean on an aquaplanet. *Journal of the Atmospheric Sciences*, *64*(12), 4270–4286. https://doi.org/10.1175/2007jas2226.1

Perez, C. L., Moore, A. M., Zavala-Garay, J., & Kleeman, R. (2005). A comparison of the influence of additive and multiplicative stochastic forcing on a coupled model of ENSO. *Journal of Climate*, *18*(23), 5066–5085. https://doi.org/10.1175/jcli3596.1

Planton, Y. Y., Guilyardi, E., Wittenberg, A. T., Lee, J., Gleckler, P. J., Bayr, T., et al. (2021). Evaluating climate models with the CLIVAR 2020 ENSO metrics package. *Bulletin of the American Meteorological Society*, *102*(2), E193–E217. https://doi.org/10.1175/bams-d-19-0337.1

Roundy, P. E. (2012). Observed structure of convectively coupled waves as a function of equivalent depth: Kelvin waves and the Madden–Julian oscillation. *Journal of Atmospheric Sciences*, *69*(7), 2097–2106. https://doi.org/10.1175/jas-d-12-03.1

Schopf, P. S., & Suarez, M. J. (1988). Vacillations in a coupled ocean–atmosphere model. *Journal of Atmospheric Sciences*, *45*(3), 549–566. https://doi.org/10.1175/1520-0469(1988)045<0549:viacom>2.0.co;2

Shi, X., Kim, D., Adames, Á. F., & Sukhatme, J. (2018). WISHE-moisture mode in an aquaplanet simulation. *Journal of Advances in Modeling Earth Systems*, *10*(10), 2393–2407. https://doi.org/10.1029/2018ms001441

Smith, R. S., Dubois, C., & Marotzke, J. (2006). Global climate and ocean circulation on an aquaplanet ocean–atmosphere general circulation model. *Journal of Climate*, *19*(18), 4719–4737. https://doi.org/10.1175/jcli3874.1

Waliser, D., Sperber, K., Hendon, H., Kim, D., Maloney, E., Wheeler, M., et al. (2009). MJO simulation diagnostics. *Journal of Climate*, *22*(11), 3006–3030. https://doi.org/10.1175/2008jcli2731.1

Wang, C. (2018). A review of ENSO theories. *National Science Review*, *5*(6), 813–825. https://doi.org/10.1093/nsr/nwy104

Wang, G., Dommenget, D., & Frauen, C. (2015). An evaluation of the CMIP3 and CMIP5 simulations in their skill of simulating the spatial structure of SST variability. *Climate Dynamics*, *44*(1–2), 95–114. https://doi.org/10.1007/s00382-014-2154-0

Weisberg, R. H., & Wang, C. (1997). A western Pacific oscillator paradigm for the El Niño-Southern Oscillation. *Geophysical Research Letters*, *24*(7), 779–782. https://doi.org/10.1029/97gl00689

Wheeler, M., & Kiladis, G. N. (1999). Convectively coupled equatorial waves: Analysis of clouds and temperature in the wavenumber–frequency domain. *Journal of Atmospheric Sciences*, *56*(3), 374–399. https://doi.org/10.1175/1520-0469(1999)056<0374:ccewao>2.0.co;2

Wu, X., Reed, K. A., Wolfe, C. L., Marques, G. M., Bachman, S. D., & Bryan, F. O. (2021). Coupled Aqua and Ridge planets in the Community Earth System Model. *Journal of Advances in Modeling Earth Systems*, *13*, e2020MS002418. https://doi.org/10.1029/2020MS002418

Yang, D., & Ingersoll, A. P. (2013). Triggered convection, gravity waves, and the MJO: A shallow-water model. *Journal of the Atmospheric Sciences*, *70*(8), 2476–2486. https://doi.org/10.1175/jas-d-12-0255.1

Zebiak, S. E., & Cane, M. A. (1987). A model El Niño–Southern Oscillation. *Monthly Weather Review*, *115*(10), 2262–2278. https://doi.org/10.1175/1520-0493(1987)115<2262:ameno>2.0.co;2